Received: 9 July 2020 | Revised: 9 November 2020 | Accepted: 1 December 2020

IET Microwaves, Antennas & Propagation

DOI: 10.1049/mia2.12095

The Institution of Engineering and Technology WILEY

ORIGINAL RESEARCH PAPER

Compact 3D-printed reflector antenna for radar applications at K-band

João R. Reis[1,2] | Carlos Ribeiro[2,3] | Rafael F. S. Caldeirinha[1,2]

[1]Instituto de Telecomunicações, Leiria, Portugal

[2]Polytechnic of Leiria, Leiria, Portugal

[3]Twevo, Lda., Coimbra, Portugal

Correspondence

João R. Reis, Polytechnic of Leiria, Leiria, Portugal.
Email: joao.reis@ipleiria.pt

Funding information

European Regional Development Fund, Grant/Award Number: Project RADAVANT (03/SI/2017 - Project n.º 033907); Fundação para a Ciência e a Tecnologia, Grant/Award Number: UIDB/EEA/50008/2020

Abstract

A compact parabolic reflector antenna aiming at radar applications in the K-band is presented. It is mainly composed of a thermoplastic material and using classical additive techniques (also known as 3D printing), the proposed high-gain antenna exhibits a novel and unique form factor, particularly of interest for applications with low payload capacity, for example unmanned aerial vehicles. The antenna is composed of four parts: (i) a paraboloid shape embodied in a supporting polylactic acid (PLA) material; (ii) a metallic coating applied to the paraboloid surface of (i), to enable it with electromagnetic reflecting properties; (iii) a PLA spacer that ensures the physical separation (i.e. focal distance) between parts (i) and (iv) and, finally, (iv) a microstrip patch antenna with a reduced ground plane to reduce feed blockage. Subsequently to an overview on the theoretical formulation of parabolic reflector antennas, an antenna targeting 20 dBi and a minimum bandwidth of 500 MHz operating in the 24 GHz ISM radar band have been dimensioned, optimised in CST Microwave Studio and validated against measurements performed on a physical prototype. The simulation and experimental results are in good agreement with the prototype yielding 18.3 dBi of gain and 2.2 GHz of useful bandwidth, clearly demonstrating the potential of the proposed antenna design.

1 | INTRODUCTION

Radio detection and ranging (radar) technology [1–3] has been extensively used over the years, since its appearance in the early 1940s [4, 5]. Since then, a long-range radar has been generically used in the military context, for target detection and recognition and air/space surveillance [1, 4]. However, with the continuous evolution of the digital era and chip integration, radar technology became rapidly available for smaller-scale applications [6–9]. Nowadays, mid- and short-range radars are widely available in the market, typically operating at micro and millimetre wave frequencies, for example, in the 24 and 77 GHz frequency bands, through commercially of-the-shelf and system-on-chip (SoC) kits [10–12]. This integration facilitates radar deployment making this technology very attractive for the automotive [13–15] and UAV markets [16–18], in particular for object detection and collision avoidance, and to assist with autonomous safety driving.

From a practical point-of-view, radar systems benefit from having high gain antennas to increase the overall system dynamic range and, consequently, the range of the radar [1–3]. Hence, typical antenna designs for radar application comprise either the use of antenna array or parabolic reflector antenna [3]. For example, parabolic reflector antennas are commonly employed in long-range radars, where very high gains and large scanning volumes are required. These characteristics, however, are challenging to mimic with antenna array limited by the feeding network, for which complexity and cost increase with the size of the array, yet providing much-limited scanning than the previous solution. Nevertheless, in mid- and short-range radars, antenna array is often preferred due to the ease of integration of microstrip technology with the printed circuit board that holds the main radar hardware. This ensures compact and lightweight form factors as it can be seen, for example, in several frequency-modulated continuous wave radar kits [10–12], where simple linear arrays of microstrip patch antennas are employed.

Some examples of parabolic reflector antenna design at micro and millimetre waves can be found in the literature [5, 19, 20–24]. In particular, the authors in [21] and further in [22]

have suggested a compact parabolic reflector design, using several layers of substrate stacked together, forming a quasi-planar parabolic dish. Even though the concept is proved successful and antenna beamsteering is also demonstrated, by displacing the feeding source from the focal point present in the top stacked layer, the antenna is cumbersome and cost-ineffective, due to the excessive number of substrate layers required to form the reflector. Alternatively, in [23, 24], the authors have successfully used 3D printing techniques to produce parabolic reflector antennas.

In fact, 3D printing antennas have become, *per se*, a hot topic in antenna design and development [23–28]. The 3D printing technology offers in general numerous advantages, such as a vast type of available printing materials with relatively strong but light-weight mechanical properties, relatively low material costs but more importantly, it allows for fast prototyping as this technique is nowadays widely available. This provides to the engineer/designer an extra degree of freedom in the design-to-product optimisation process, as a prototype is quickly obtained and less costly, e.g. when comparing with other manufacture techniques as machining or moulding. Particularly in antenna engineering [23–28], 3D printing can be explored in the design of reflectors [23, 24], dielectric lens [25, 26], as dielectric substrate [27, 28], or to explore other alternative shapes and forms that would not be easily achieved with regular substrates. The major downside of the 3D printing is the resolution associated with the additive manufacturing (layer composition). This could create some imperfections in the printed parts, although printing resolution could be as low as 0.1 mm (depending on the printer accuracy), and a surface optimisation can be done with filler material and fine sanding.

Particularly in [23], the authors remarkably designed and manufactured a dual-band circularly polarized offset stepped-reflector antenna at K and Ka bands, respectively. The antenna, composed of a reference feeding horn and a 3D-printed stepper reflector, was produced in nylon-polyamide material and spray-painted with a silver-based component to make it reflective. The dual-band operation is ensured by the stepped reflector, which consists of four co-focal paraboloids with specific focal lengths, ensuring constructive interference at the respective frequencies of operation. Experimental work carried out on the prototype reports a peak directivity of around 37 and 40 dB at 20 and 30 GHz, respectively. In [24], a 3D printed parabolic reflector antenna is proposed in the Ka-band. The reflector, printed in polylactic acid (PLA) material, is covered with several layers of copper tape with a conductor thickness of 4 mm, to ensure reflecting properties. A maximum gain of around 28 dBi has been reported at 30 GHz, using a conical horn antenna as feeding source.

To this extent, the authors present a compact parabolic reflector antenna, designed based on thermoplastic materials and using 3D printing technology, for radar (and radio communication) applications operating in the 24 GHz ISM radar band. This work builds upon the one presented by the authors in [29]. The proposed antenna model, depicted in Figure 1, exhibits a novel and unique form factor in which the feeding element is co-allocated in the same block as the parabolic reflector, yielding a compact monoblock shape. This withdraws the spacing and weight issues typically associated when using horn antennas (and subsequent mechanical supports) as feeding source of a reflector antenna, as in [23, 24]. Besides being to be easy to produce and affordable, as the base material is fused plastics manufactured using additive printing, the proposed antenna is also compact and light-weight, ideal for applications with low payload capacity, for example in unmanned aerial vehicles (UAVs). Therefore, an overview of the main parabolic reflector antenna parameters is performed, to assist with the design of the proposed antenna. Subsequent design, simulation, optimisation and validation against experiments on a physical prototype are also presented.

This study is organized as follows: Section 2 gives an overview of the main parabolic reflector parameters, including a design guideline to assist with the antenna dimensioning. Section 3 gives details about project specification, including the target operative parameters of the antenna, supporting materials, and the techniques used in antenna manufacture. The setup used for the experimental characterization is also described in this section. In Section 4, the monoblock antenna is simulated, optimised, constructed and experimentally validated. Simulation and experimental results are presented side-by-side and followed by a critical discussion. Finally, the main conclusions are drawn in Section 5.

2 | OVERVIEW OF PARABOLIC REFLECTOR ANTENNA

Despite being well documented in many textbooks [1–3] and thoroughly analysed by the authors in [29], this section covers the main attributes of parabolic reflector antennas leading towards the elaboration of a design guideline to further assist in the elaboration of a table comparing the theoretical, simulated and experimental results, presented in Section 4.

2.1 | Main design parameters

The underlying principle of a parabolic reflector is depicted in Figure 2. A feed source distanced at a focal distance F, illuminates a parabolic reflector with diameter D and depth C, which in turn redirects (reflects) the incident spherical wave (near-field interaction) to yield far-field distance immediately off the reflector, improving therefore the antenna effective aperture and consequently its gain.

In fact, the diameter D, depth C and focal distance F are the main physical parameters necessary to define the shape of a parabolic reflector, typically related by a focal-length-to-diameter (F/D) ratio, which can be expressed by Equation (1)

$$C = \frac{D^2}{16F} = \frac{D}{16(F/D)} \tag{1}$$

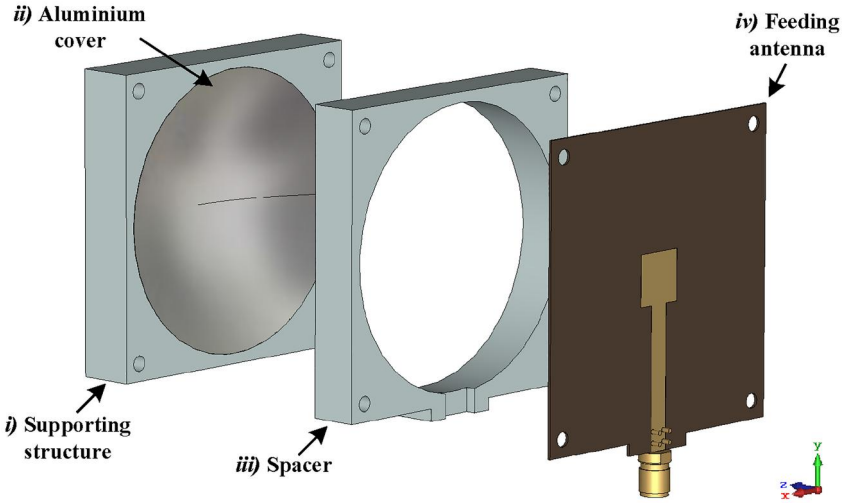

FIGURE 1 Block diagram of the proposed antenna configuration

Following [30], the gain (in dB) of parabolic reflector antenna, in closed form, is expressed by Equation (2)

$$G = 10\log_{10}\left[\eta\left(\frac{\pi D}{\lambda}\right)^2\right], \quad where\ \eta = \eta_s\eta_t\eta_p\eta_b\eta_r, \qquad (2)$$

where D is the diameter of the reflector, λ is the operating wavelength and η is the aperture efficiency. The aperture efficiency can be defined as the relation of the actual gain to the maximum theoretical gain achievable for the same aperture area [3]. Thus, it is a measure that relates the spillover efficiency—η_s; the taper or illumination efficiency—η_t; the phase efficiency—η_p; the feed blockage efficiency—η_b and finally, η_r—random error efficiency, associated with the reflector surface irregularities [3]. Each of the factors introduced above has significant effect on the total efficiency η and thus in gain. Typical values for aperture efficiency vary between 0.3 and 0.7 [3], for a parabolic reflector configuration as the one represented in Figure 2.

According to several textbooks [1, 3], not all the efficiency parameters presented above have the same weight, in global aperture efficiency η. The ones that contribute the most are spillover (η_s) and taper efficiencies (η_t), which are associated with the radiation pattern of the feeding antenna and how well it is matched to the reflector. Hence, the reflector design problem consists mostly of matching the feed antenna pattern to the reflector shape and a compromise between spillover and taper efficiency must exist. For example, very high spillover efficiency can be achieved by a narrow beam pattern with low minor lobes at the expense of a very low taper efficiency [3]. Nevertheless, the traditional rule of thumb for this trade-off is that the best efficiency occurs when the illumination at the edge of the parabolic reflector is 10 dB down relative to the one at the centre [1]. However, the 10 dB rule is just a practical consideration that ultimately will depend on the directivity of the feeding source and may not be respected (e.g. dipole antenna used as feeding source [3]).

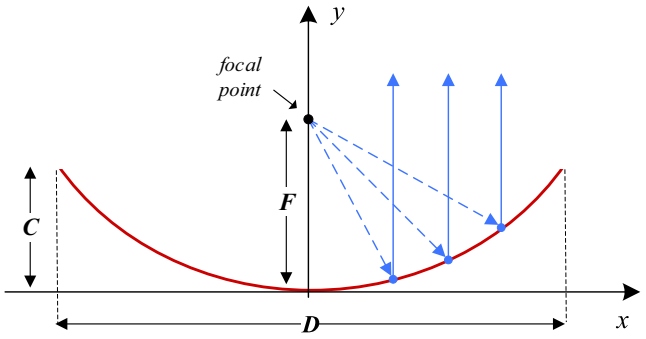

FIGURE 2 Generic block diagram of a parabolic reflector antenna

Thus, to best match parabolic reflector to the feeding antenna, Equation (3) relates the edge direction θ_{max}, i.e. direction of the feeding antenna radiation pattern in which the gain is 10 dB lower than at boresight, with the F/D ratio of the parabolic reflector.

$$\theta_{max} = 2\tan^{-1}\left(\frac{1}{4(F/D)}\right) \qquad (3)$$

Finally, another parameter that can be estimated from the physical properties of the reflector is the half-power beamwidth (HPBW). According to [30], an approximation the HPBW can be obtained using Equation (4)

$$\text{HPBW} = 70\frac{\lambda}{D} \qquad (4)$$

2.2 | Suggested design guideline

According to the considerations specified in the previous section, this study follows the subsequent guideline, which will assist with the antenna designs being presented in Section 4:

1. Obtain the reflector diameter using (2) for the desired gain. Since the efficiency is not known at this point, an initial efficiency of $\eta = 0.5$ can be considered;
2. Analyse the radiation pattern of the feeding antenna. Obtain the direction in degrees, in which its gain is 10 dB lower than at boresight. Use the angle to find the F/D ratio through (3); and
3. Calculate the focal distance F through the F/D ratio and the reflector depth C, using Equation (1).

3 | MONOBLOCK ANTENNA DESIGN CONSIDERATIONS

3.1 | Proposed antenna configuration

The antenna configuration proposed here is depicted in Figure 1. The antenna is composed of four parts: (i) a paraboloid shape engraved in thermoplastic material, produced using 3D printing technology; (ii) a metallic coating layer applied to (i) to enable it with EM reflecting properties; (iii) a spacer that ensures the distance between part (i) and (iv) (i.e. focal distance) and, finally, (iv) an enhanced microstrip patch antenna with reduced ground planned used as feeding source. This configuration results in a compact, a monoblock, form factor which is sought to be robust and lightweight due to the properties of the thermoplastic materials typically utilised in the 3D printing.

In particular, the antenna is designed to meet the requirements of the following specifications: (i) frequency of operation at 24.125 GHz, corresponding to the central frequency of the 24 GHz ISM radar band; (ii) a bandwidth (BW) of (at least) 500 MHz, to cover the entire announced frequency band and (iii) a total gain of 20 dBi, while keeping the side-lobe level (SLL) below 12 dB.

Details about design, simulation, optimisation and experimental characterisation are included in Section 4.

3.2 | Supporting structure material

The supporting parts of the proposed antenna, that is, paraboloid main body and spacer (parts (i) and (iii) of Figure 1, respectively), are constructed using additive manufacturing. Although any other thermoplastic material could have been selected, e.g. acrylonitrile butadiene styrene (ABS), this antenna was specifically designed and optimised for PLA, as it is one of the easiest materials to print with, affordable and widely available in the market. PLA is a thermoplastic polymer derived from renewable raw materials such as corn starch and sugarcane, which are fermented to lactic acid [31] offering, however, comparable properties, for example, stiffness, to other plastics in the industry.

Although widely used in 3D printing, the dielectric properties of the PLA material supplied by the manufacturers are often characterized at very low frequencies (around 1 MHz) and, thus, not in line with the frequency range of this work. To this end, a literature survey was performed with the aim of finding the dielectric properties of the PLA material at micro/millimetre wave frequencies. According to the survey, summarized in Table 1, an $\epsilon_r = 2.75$ and a $\tan(\delta) = 0.02$ was found to be a common value among the scientific community, for the electrical properties of this material, at microwave frequencies. This study was intentionally performed a priori so that realistic values of the PLA material could be taken into consideration in the electromagnetic (EM) simulations and counted the global antenna performance.

At the time of prototyping, PLA from BQ (grey colour) [32] has been extruded with a 0.4 mm nozzle at 220° (hot-end temperature), using a Creality Ender 3 printer, to produce the plastic parts of the antenna (parts i and iii) of Figure 1). All the parts were prototyped considering 0.2 mm of layer height and 50% infill. Nevertheless, to ensure an even and smooth surface and eliminate any roughness associated with layering that could impact electromagnetic performance, all the 3D printed parts were fine sanding prior to prototype assembly. To evaluate the printer accuracy, several prototypes of both the parabolic parts (i and spacer part iii) of Figure 1 have been built and the process repeatability was found to be within +/0.05 mm tolerance.

3.3 | Parabolic surface metallisation

To enable the imprinted paraboloid shape (part i) of Figure 1) with electromagnetic reflecting properties, its surface was metallised with aluminium alloy. In the simulation environment, this is set by considering an extra paraboloid solid with finite thickness to represent the metallic layer. The thickness of the solid was considered to be 20 μm, exceeding therefore the skin depth of $\delta_s = 0.55$ μm for the aluminium (for a conductivity $\sigma = 3.56 \times 10^7$ S/m). The skin depth was calculated using the generic formula that can be found, e.g. in [3]. In the prototyping stage, the metallisation was done stamping two layers of aluminium foil with an approximate thickness of 20 μm, to ensure good shielding, trimmed and moulded to the shape of the parabolic surface.

TABLE 1 Dielectric properties of PLA material

ϵ_r	Tan (δ)	Freq. range*	Reference
2.75	0.05	0–20 GHz	[33]
≈ 2.75	NA	1 kHz–3 GHz	[34]
2.72	NA	12–18 GHz	[25]
2.71	0.017	1–10 GHz	[35]
2.57–2.72	0.01	30–50 GHz	[36]
2.68	0.0235	4.38 GHz	[37]
2.54	0.019	40 GHz	[31]
2.75	0.02	22–26 GHz	Considered in this work

*Frequency range considered in the work.

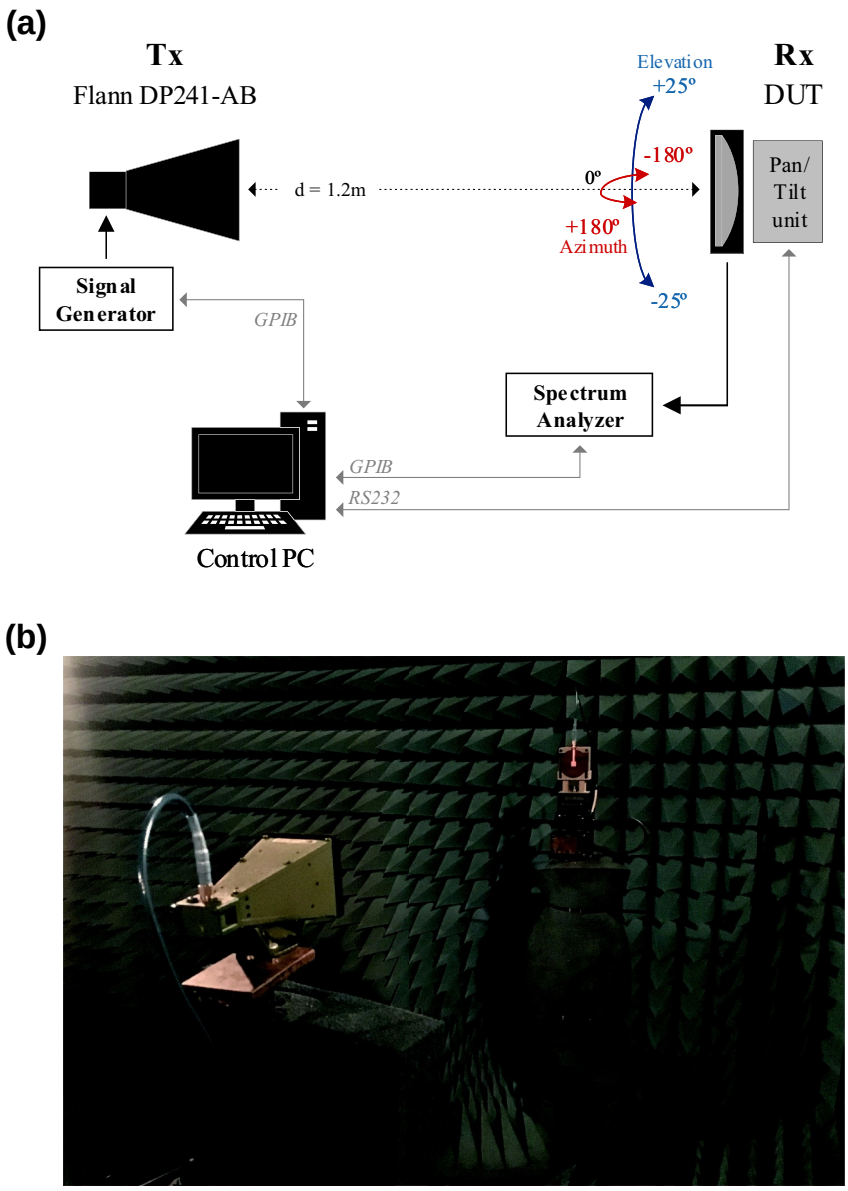

FIGURE 3 Experimental setup: (a) side-view representation and (b) photography of the setup inside the anechoic chamber

3.4 | Experimental setup

To test and characterise the proposed antenna model, a prototype of the monoblock antenna has been built and evaluated inside an anechoic chamber. In particular, the antenna matching ($S_{1,1}$) and radiation patterns in the two main antenna planes have been measured. While the $S_{1,1}$ was obtained on the bench, using a PNA-X Network Analyser (Agilent N5242A), from 22 to 26 GHz, the antenna radiation patterns were measured using the setup of Figure 3(a).

At the transmitter side, a well-characterized horn antenna (Flann microwave DP241) was connected to a signal generator (R&S SMR27), producing a continuous wave (CW) signal with 10 dBm, ranging from 23.5 to 25.5 GHz, with 12.5 MHz steps. At the receiver end, a well-characterized standard gain horn antenna (Flann microwave 20240-20) was used as reference [and later replaced by the antenna under test (AUT)]. The receiver antenna was connected to a Spectrum Analyser (Agilent E4407B) to measure the received power. Both antennas were located 1.2 m apart to ensure that the measurements are performed in the far-field region.

To obtain the radiation pattern in the two principal antenna planes, the transmitter antenna was kept fixed throughout the measurements, while the receiver one was made to rotate around its own axis, with the assistance of motorized pan/tilt head unit. At each angular step within the range of $-180° \leq Az \leq 180°$ and $-90° \leq El \leq 90°$, the received power was acquired and referenced to the absolute gain of the receiver standard gain horn antenna, following the gain transfer method procedure described in [38]. Prior to the measurement, antennas were aligned to the maximum power direction.

The synchronization between the signal generator and spectrum analyser, data acquisition and movement control, was executed in Matlab using an in-house software routine. To avoid

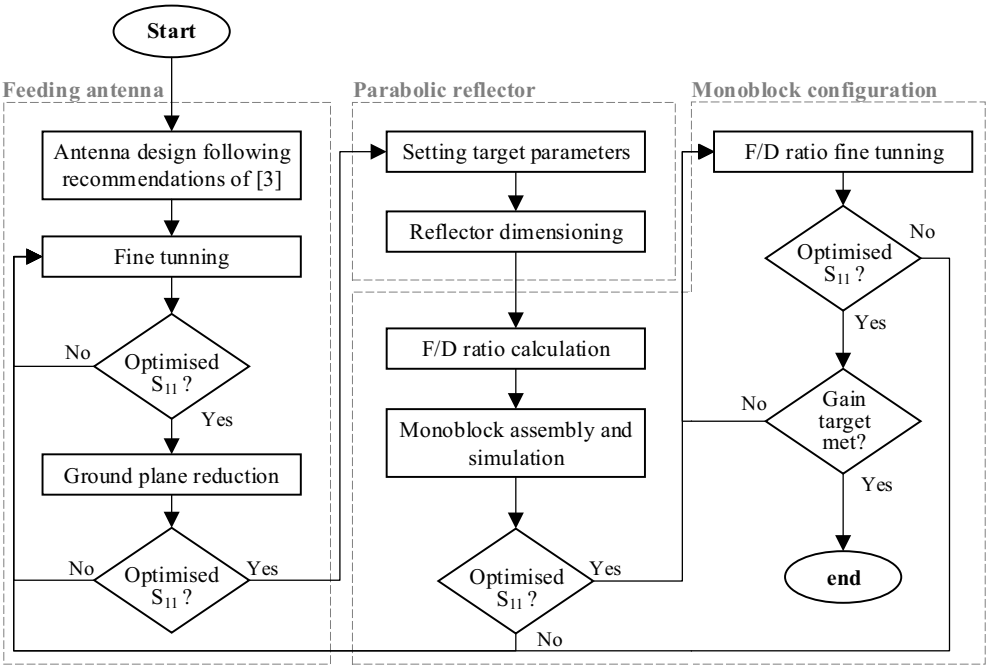

FIGURE 4 Flow chart of the monoblock antenna optimisation process

any external electromagnetic contamination and to obtain precise and clean measurement results, all the measurements were obtained inside an anechoic chamber (Figure 3(b)).

4 | SIMULATION, PROTOTYPING AND CHARACTERIZATION

4.1 | Feeding antenna

To implement the feeding element of the monoblock antenna, a microstrip patch was considered. This particular feed design was selected due to its planar form factor, simple manufacturer process and low production cost, which is in line with the concept of the proposed antenna. Moreover, since its radiating properties can be manipulated by slightly changing/optimising the design, for example, radiation pattern shape, it can be easily adapted to the reflector shape. In fact, the optimisation procedure considered for the implementation of the monoblock antenna is summarised in Figure 4 and well detailed throughout this section.

Accordingly, the layout of Figure 5 has been etched on a double-sided Rogers RT5880 substrate, with $\epsilon_r = 2.2$, $\tan\delta = 0.0009$ and dimensions of $60 \times 60 \times 0.508$ mm^3. The feed follows the design recommendations of [3] for a microstrip patch antenna, but optimised for a minimal ground plane, to reduce feed blockage of the final antenna configuration.

In the top plane (Figure 5(a)), a 50-Ω feed line with length F_l and width F_w, insets the top patch defined by $T_w \times T_l$ by I_l, connecting it to an SMA connector placed at the bottom edge of the substrate. In turn, a microstrip to coplanar waveguide (CPW) transition has been employed to match the feeding line to the SMA connector. In the bottom part (Figure 5(b)), the ground plane defined by a $B_w \times B_l$ patch and a G_l and G_w line was considered. The shape of the ground plane was achieved by parametrically reducing, in simulations, the dimensions of the bottom patch and trace width so that the initial antenna impedance (and thus the S_{11}) given by the theoretical formulation of [3] would not be impacted. Moreover, a vertical offset of the $B_w \times B_l$ patch is considered, in relation to the top one that is centred with the substrate, to compensate for the impact of the extended feed line design in the final radiation pattern shape.

After an initial fine-tuning in CST MWS, to set the resonant frequency of the feeding antenna at 24.125 GHz, the following antenna dimensions were obtained: $T_w = 4.92$ mm, $T_l = 3.95$ mm, $I_w = 2.06$ mm, $I_l = 1.35$ mm, $F_w = 1.56$ mm, $F_l = 24$ mm, $c_t = 1.6$ mm, $c_l = 4.7$ mm, $c_w = 1.25$ mm, $c_g = 0.2$ mm, in the top plane and, $B_w = 10$ mm, $B_l = 11$ mm, $G_w = 4$ mm, $G_l = 28$ mm, in the bottom plane and, a vertical offset of 1 mm between patches. The simulation exhibits the S_{11} parameter depicted in Figure 6(a) (blue dash curve). According to the results, the antenna is resonating at 24.125 GHz, presenting a relatively good impedance matching for the frequency range defined between 23.7 and 24.55 GHz, i.e. $S_{11} < -10$ dB, yielding a bandwidth of approximately 850 MHz (3.5%).

However, when the entire antenna structure was placed together, that is, trimmed microstrip antenna optimised at 24.125 GHz + spacer + parabolic reflector (as in Figure 1), it was found that the overall S_{11} was slightly above the recommended 10 dB threshold, as depicted in the blue dashed line of Figure 6(b). This effect is sought to be related to impedance mismatch caused by insertion of the reflector in front of the feeding antenna enclosed by the PLA spacer. Thus, an optimisation of the parameters T_w, I_w, F_w and B_l was performed, with the goal of reducing the overall S_{11} to below 10 dB, and

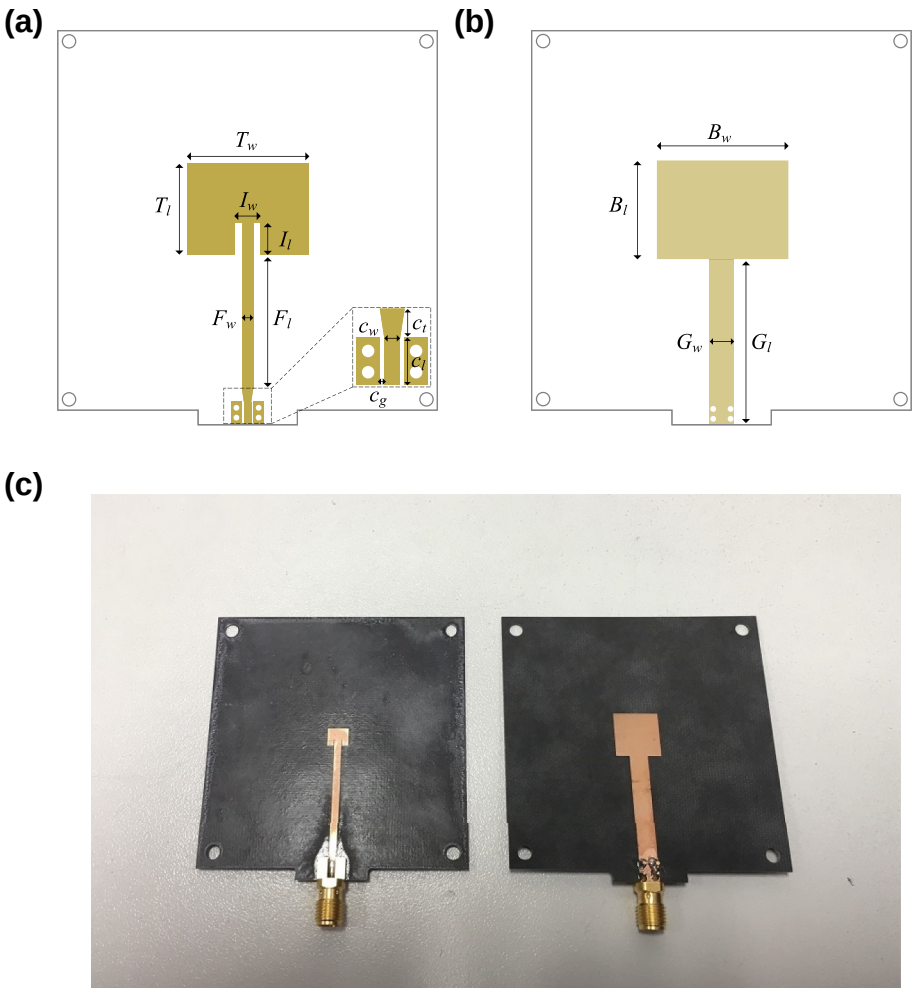

FIGURE 5 Feeding microstrip patch antenna: (a) top and (b) bottom layer representation (dimensions represented out of scale) and (c) photography of the prototyping

consequently, increase the final effective bandwidth. After optimisation, it was found that the values of $T_w = 4.75$ mm, $I_w = 1.94$ mm, $F_w = 1.54$ mm and $B_l = 10$ mm would allow for a better overall S_{11} response, as depicted in Figure 6(b) (orange-dotted curved). This design adjustment led to a consequent shift of +225 MHz in the resonant frequency of the feeding antenna (when analysed as an individual), as it can be observed in Figure 6(a) (orange-dotted curve). Thus, the final feeding design presents a bandwidth of 960 MHz (3.9%) resonating at 24.35 GHz, which compares to the measured bandwidth of 1.37 GHz and the resonance frequency of 24.28 GHz (red-filled curve), obtained on the physical prototype of Figure 5(c). The minor discrepancy in S_{11} parameter between simulations and experiments is sought to be associated with the effect of a protective anti-corrosive layer applied to the prototype not considered in simulations.

At the project frequency, that is, 24.125 GHz, the feeding antenna exhibits then a maximum absolute gain of around 7.7 dBi in simulation and 7.5 dBi in experiments realized on the prototype, as it can be seen in the radiation patterns of Figure 7. In fact, the experimental and simulated radiation patterns cuts in the main antenna planes are in relatively good agreement. In the elevation plane (Figure 7(b)), while the HPBW is of 70° in both simulations and experiments, the θ_{max} is set at ± 80° and ± 83° in simulation and experiments, respectively. Nevertheless, in the azimuth plane, the half-power beam width (HPBW) is 76° in both simulation and experiments, as depicted in Figure 7(a). Furthermore, the θ_{max} direction is verified at ±75° in simulation and at ±72° in experiments. For this plane, in particular, the level of the higher side-lobe, i.e. the SLL, is −22 dB verified in simulations against −10 dB obtained with measurement. This difference is sought to be caused by the mechanical rig utilised to support the patch antenna to the pan/tilt unit, not taken into account in the simulation environment.

4.2 | Monoblock antenna

To build the monoblock antenna suggested in this study (Figure 1) and meet the project specifications well defined in Section 3.1, a parabolic revolution with 56 mm of diameter has

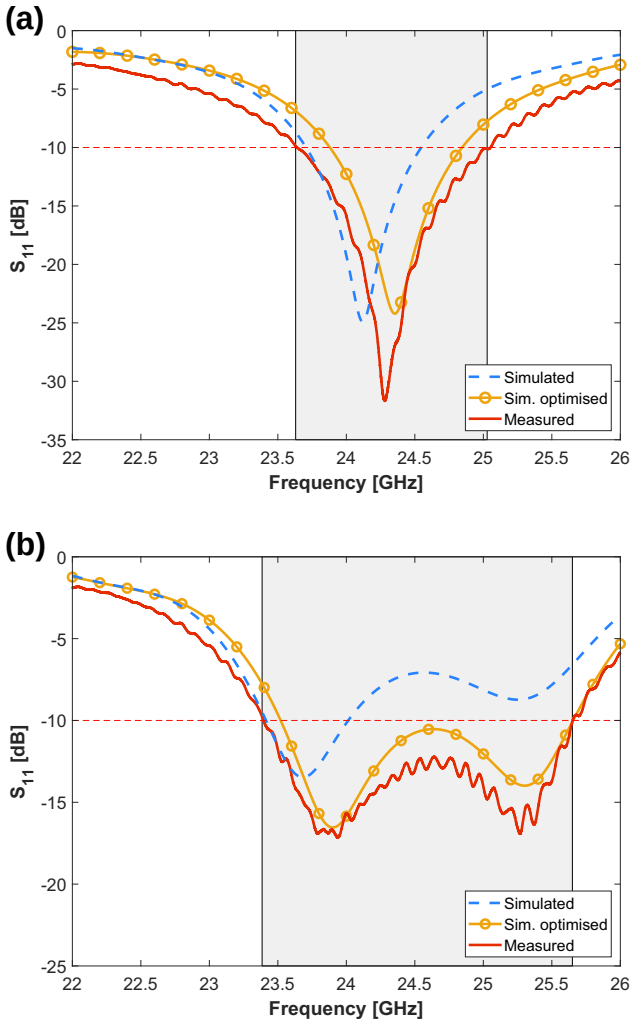

FIGURE 6 Simulated and measured S_{11} parameters for (a) feeding antenna and (b) monoblock antenna configuration

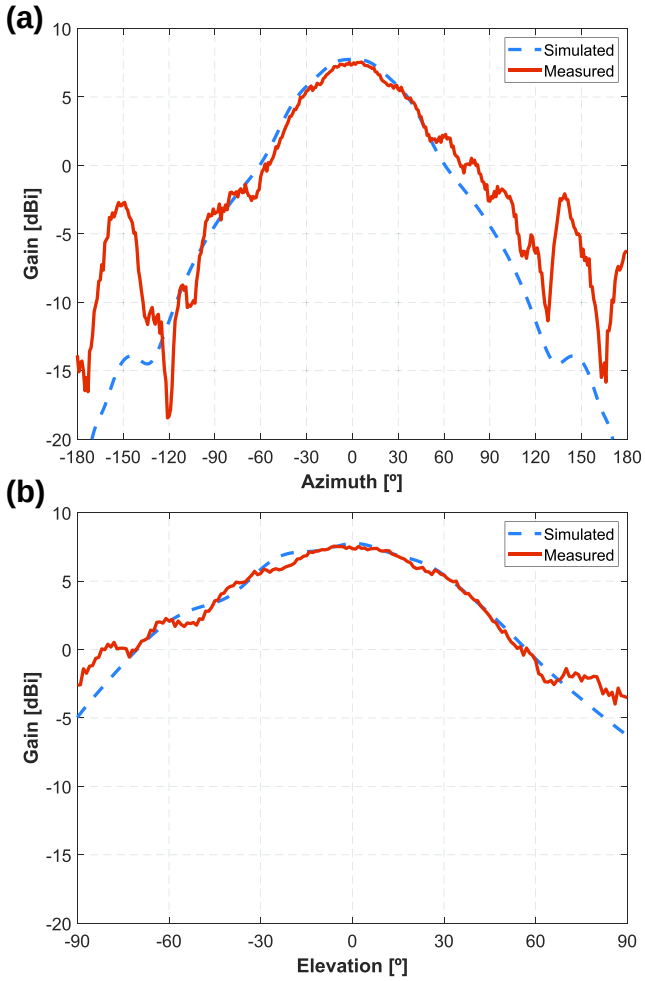

FIGURE 7 Simulated and measured radiation pattern for the feeding antenna, in the two main antenna planes, at 24.125 GHz

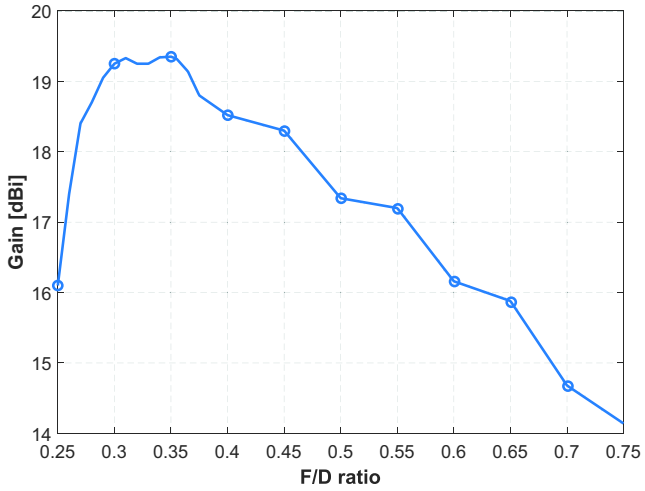

FIGURE 8 Simulated F/D ratio variation for a parabolic reflector with $D = 56$ mm at 24.125 GHz

been considered. The diameter of the parabola was obtained from Equation (2) with $\eta = 0.5$, to achieve 20 dBi of gain. An F/D ratio of 0.35 has been used to best match the parabolic shape to the microstrip feeding antenna, conferring to the design a theoretical focal distance of 19.6 mm. This F/D ratio value was initially estimated through Equation (3), considering the experimental θ_{max} for the azimuth plane of 72°(obtained in Section 4.1). However, a parametric simulation carried out in CST (Figure 8) indicated that the maximum gain of the arrangement was 19.5 dBi, obtained for an F/D of 0.345. This F/D ratio would result then in a focal distance of 19.3 mm not possible be physically achieved due to the printer resolution (0.2 mm layer). Hence, the F/D = 0.35 ratio obtained from theoretical formulation was considered, highlighting one of the disadvantages of the 3D printing process in antenna design as, in this particular case, printer resolution may affect antenna performance, especially due to the difficulty of setting separation distances not multiple of the layer resolution.

A paraboloid shape with 56 mm of diameter and 10 mm deep has been embodied in a 60 × 60 × 11 mm^3 solid of PLA material and further metallised to enable the reflection of the EM waves. Aluminium material was then applied to the paraboloid surface as described in Section 3.3. A hollow PLA

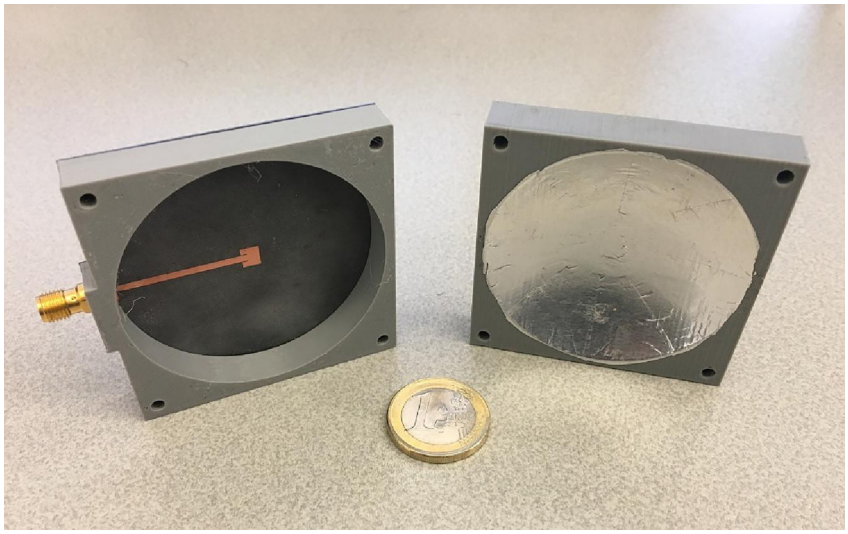

FIGURE 9 Prototype of the monoblock antenna

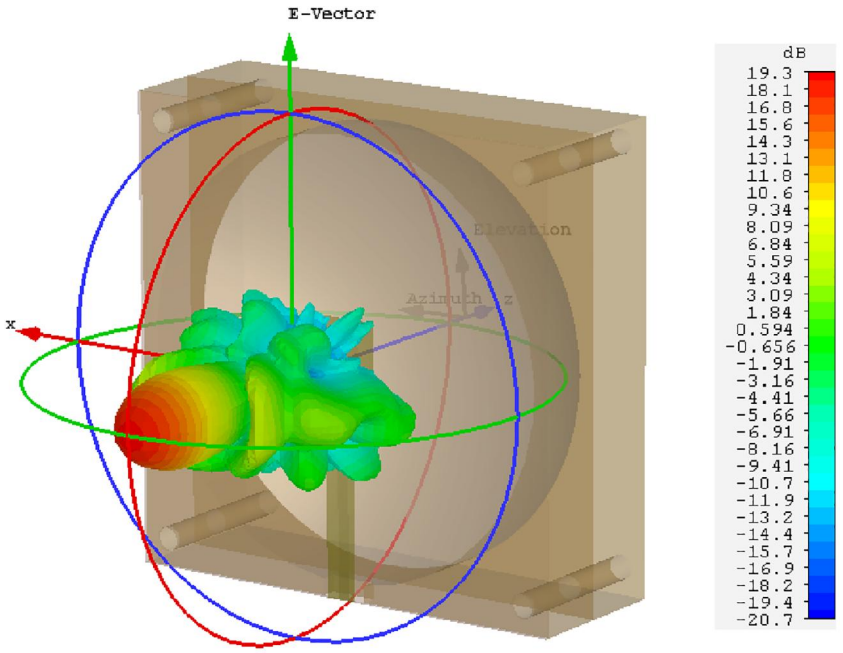

FIGURE 10 Simulated 3D radiation pattern of the monoblock antenna

spacer with dimensions of 60 × 60 mm^2 and 9.6 mm of thickness has been used to ensure the desired physical separation between the reflector and the feeding antenna, that is, focal distance. The spacer was trimmed out internally, with the same diameter as the parabola, to remove the excess material. Four holes have been considered at each corner of the antenna to enable stacking of all antenna parts. Nylon screws have been used to fix all the parts together, but not considered in simulations. The proposed monoblock antenna, which exhibits an overall dimension of 60 × 60 × 21.1 mm^3, was then simulated in CST MWS and prototyped using addictive manufacture techniques, as detailed in Section 3.2. The prototype of the monoblock antenna is depicted in Figure 9.

The simulated and experimental S_{11} parameters for the monoblock antenna are depicted in Figure 6(b). After the feeding optimisation performed in Section 4.1, the antenna presents a relatively good impedance matching, with an $S_{11} < -10$ dB within the frequency band defined from 23.5 to 25.6 GHz (BW = 2.1 GHz—8.5%) in simulation (orange circled curve) and from 23.4 to 25.6 GHz (BW = 2.2 GHz—8.9%) obtained in the prototype (red fill curve). This represents a substantial improvement over the antenna bandwidth prior to the feeding optimisation.

According to the radiation patterns of both Figures 10 and 11, a maximum gain of 19.3 dBi and an HPBW of 16°, in both azimuth and elevation planes, are obtained at 24.125 GHz. In the prototype, an absolute gain of 18.3 dBi and an HPBW of 16° and 14° in the azimuth and elevation planes, respectively, are measured. Furthermore, the SLL (to the higher side-lobe) is −13.7 dB in simulation against −14.4 dB

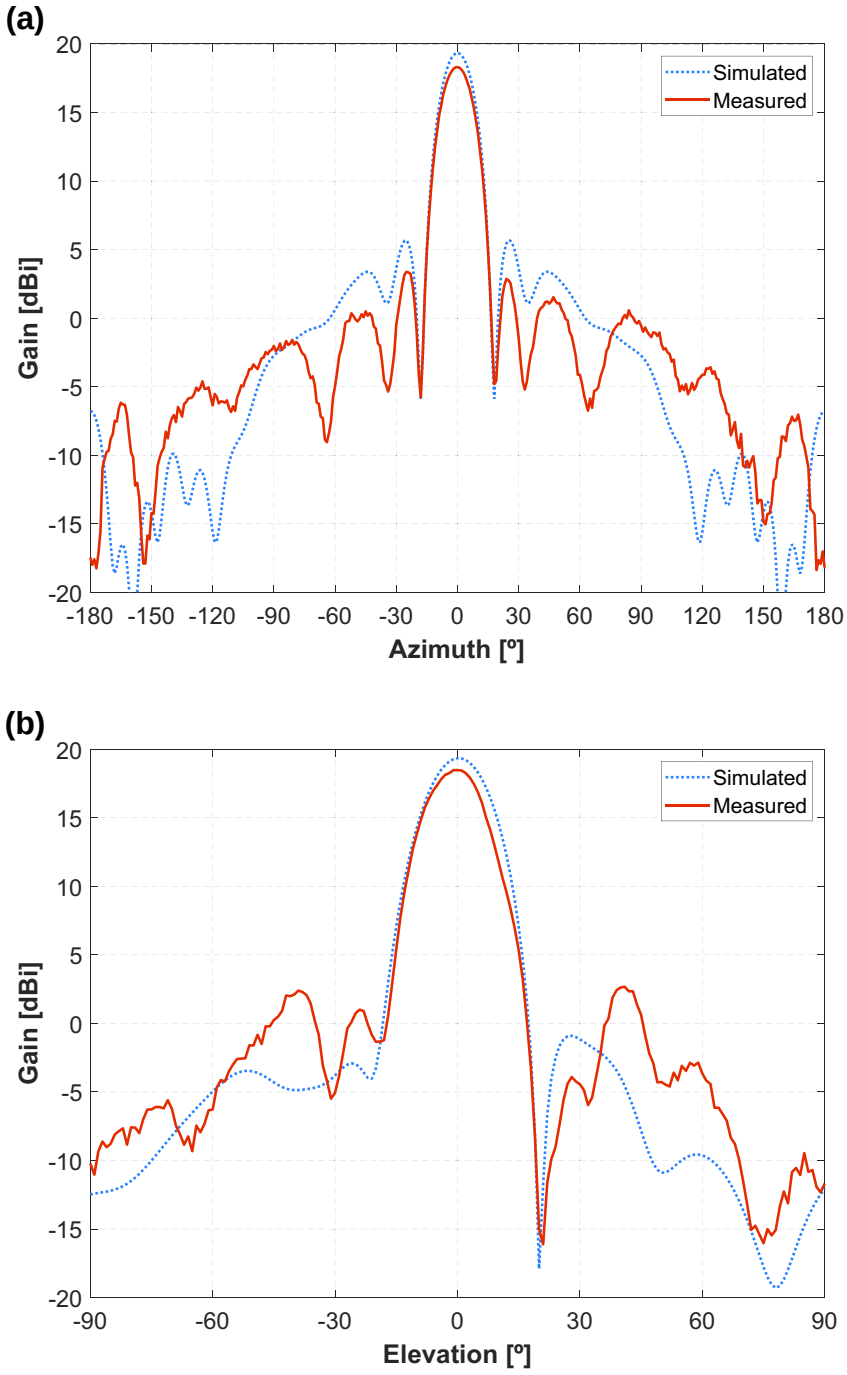

FIGURE 11 Simulated and measured radiation pattern for the monoblock antenna configuration in (a) azimuth and (b) elevation planes at 24.125 GHz

obtained with the prototype. The similarity between simulated and experimental results is notorious, validating therefore the proposed antenna model. However, the differences experienced in gain between the simulated and experimental results could be related to losses in the SMA connector, which was not considered for simulation, but also due to the small imperfections on the reflector caused by the manual metallisation process (surface roughness). Such imperfections may impact the performance of the antenna, as surface roughness is also one of the input parameters of aperture efficiency (as seen in Section 2), impacting the global aperture efficiency and thus the gain.

Nevertheless, when analysing in detail the radiation pattern in the azimuth plane (Figure 11(a)), an unexpected back-lobe with −7 dBi of gain is presented in simulation. Although this back-lobe is attenuated by 26 dB relative to the maximum of the radiation pattern and could be neglected, this may suggest that some energy was still passing through the metallised surface, despite the fact the thickness of the considered metallic surface exceeds by ×40 the skin depth of the aluminium, as detailed in Section 3.3. This situation is not verified in the measurement results, where the front-to-back ratio is 35 dB, ensuring that a good metallisation of the parabolic surface was performed.

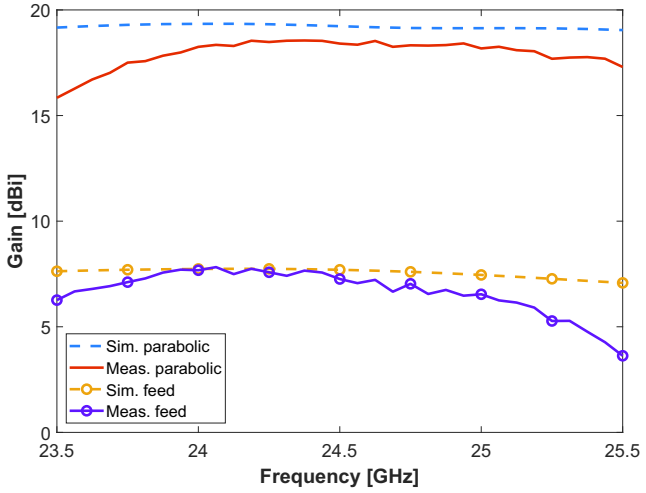

FIGURE 12 Comparison of the simulated and experimental gain over the frequency

Over the useful antenna bandwidth (23.5–25.5 GHz) that covers the 24 GHz ISM radar band in which the monoblock antenna was designed to operate, the total gain presents a smooth linear response. According to the measurements, the gain only decays 2.5 dB relative to the maximum absolute gain of 18.6 dBi found at 24.35 GHz as observed in Figure 12. This in fact represents an average gain of around 10 dB when comparing the microstrip patch feeding antenna against the monoblock configuration, clearly demonstrating the potential of the proposed antenna design.

In summary, the main performance parameters of the monoblock antenna are detailed in Table 2, comparing side-by-side the analytical against simulations and experiments results realized on a physical prototype of the monoblock antenna at the project frequency (24.125 GHz).

TABLE 2 Main monoblock antenna parameters at the project frequency (24.125 GHz)

Parameter	Target†	Simulated	Measured	Units
Gain	20	19.3	18.3	[dBi]
BW	0.5	2.1	2.2	[GHz]
HPBW in azim.	15.5‡	16	16	[°]
HPBW in elev.	15.5‡	16	14	[°]
SLL	−12	−13.7	−14.4	[dB]
App. efficiency (η)	0.5	0.44	0.34	n/a

†Set by the project specification/ requirements;
‡Extracted analytically using Equation (4).

5 | CONCLUSIONS

The authors present a compact, high-gain, monoblock antenna, designed to operate in the 24 GHz ISM radar band. The antenna is mostly constructed based on thermoplastic materials produced using addictive manufacturer techniques, configuring a novel approach in antenna design. Firstly, an overview of the main parabolic reflector parameters is performed, yielding to the elaboration of a design guideline to assist with the proposed antenna dimensioning. Subsequently, the main project considerations are specified including the operative parameters of the antenna, supporting material and its characterization and the techniques used in antenna manufacture. The setup used for the experimental characterization is also described. Finally, the proposed antenna is designed, optimised, constructed and experimentally validated, starting with the feeding antenna, that is, a microstrip patch with the reduced ground plane, and concluding with the overall monoblock antenna configuration. Simulation and experimental results, which are in good agreement, are presented side-by-side and critically discussed. The proposed antenna model, with an overall dimension of 60 × 60 × 21 mm^3, presents according to the experiments about 18.3 dBi of gain at 24.125 GHz, a total bandwidth of 2.2 GHz, an HPBW of 16° and 14°, in the azimuth and elevation planes, respectively, and a maximum SLL level of −14 dB. Further work will aim at the study of novel techniques and materials for prototyping improvement and particularly for surface metallisation, while keeping the unique, compact, and innovative shape that can be easily adaptable to any radar and radio communications system and employed in systems with limited payload capability.

ACKNOWLEDGEMENTS

This work was partially supported by the European Regional Development Fund (FEDER), PO CENTRO/SI-IDT, Project RADAVANT (03/SI/2017—Project no.° 033907) and by the Portuguese Government, Foundation for Science and Technology, FCT, through the financial support provided under UIDB/EEA/50008/2020.

ORCID

João R. Reis https://orcid.org/0000-0002-0356-9839
Rafael F. S. Caldeirinha https://orcid.org/0000-0003-0297-7870

REFERENCES

1. Skolnik, M.I.: Radar Handbook. In: Electronics Electrical Engineering, 3rd ed., McGraw-Hill Education, New York (2008)
2. Mervin, C., Budge, S.R.G.: Basic Radar Analysis (Artech House Radar). Artech House Publishers, Norwood (2015)
3. Balanis, C.A.: Antenna Theory: Analysis and Design, 4th ed., John Wiley & Sons, New York (2016)
4. Guarnieri, M.: The early history of radar [Historical]. IEEE Ind. Electron. Mag. 4(3), 36–42 (2010)
5. Cutler, C.C.: Parabolic-antenna design for microwaves. Proc. IRE. 35(11), 1284–1294 (1947)
6. Li, C., et al.: A review on recent progress of portable short-range noncontact microwave radar systems. IEEE Trans. Microw. Theory Tech. 65(5), 1692–1706 (2017)
7. Öztürk, E., et al.: A 60-GHz SiGe BiCMOS monostatic transceiver for FMCW radar applications. IEEE Trans. Microw. Theory Techniq. 65(12), 5309–5323 (2017)
8. Pyo, G., et al.: Single-antenna FMCW radar CMOS transceiver IC. IEEE Trans. Microw. Theory Techn. 65(3), 945–954 (2017)

9. Peng, Z., et al.: A portable FMCW interferometry radar with programmable low-IF architecture for localization, ISAR imaging, and vital sign tracking. IEEE Trans. Microw. Theory Tech. 65(4), 1334–1344 (2017)
10. DEMO DISTANCE2GO—Infineon Radar Demo Board. https://www.infineon.com/cms/en/product/evaluation-boards/demo-distance2go/ (2019). Accessed 10 April 2020
11. DEMO SENSE2GOL—Infineon radar demo board. https://www.infineon.com/cms/en/product/evaluation-boards/demo-sense2gol/ (2019). Accessed 10 April 2020
12. AWR1642 Single-chip 76-GHz to 81-GHz Automotive Radar Sensor. https://www.infineon.com/cms/en/product/evaluation-boards/demo-sense2gol/ (2019). Accessed 10 April 2020
13. Schneider, M.: Automotive radar: status and trends. In: Proceedings of the German Microwave Conference GeMIC, pp. 144–147 (2005)
14. Menzel, W., Moebius, A.: Antenna concepts for millimeter-wave automotive radar sensors. Proc. IEEE. 100(7), 2372–2379 (2012)
15. Chipengo, U.: Full physics simulation study of guardrail radar-returns for 77 GHz automotive radar systems. IEEE Access. 6, 70053–70060 (2018)
16. Patel, J.S., et al.: Review of radar classification and RCS characterisation techniques for small UAVS or drones. IET Radar Sonar Navig. 12(9), 911–919 (2018)
17. García Fernández, M., et al.: Synthetic aperture radar imaging system for landmine detection using a ground penetrating radar on board a unmanned aerial vehicle. IEEE Access. 6, 45100–45112 (2018)
18. Lort, M., et al.: Initial evaluation of SAR capabilities in UAV multicopter platforms. IEEE J. Sel. Top. Appl. Earth Obs. Remote Sens. 11(1), 127–140 (2018)
19. Mehrabani, A., Shafai, L.: Compact dual circularly polarized primary feeds for symmetric parabolic reflector antennas. IEEE Antennas Wirel. Propag. Lett. 15, 922–925 (2016)
20. Manohar, V., et al.: Synthesis and analysis of low profile, metal-only stepped parabolic reflector antenna. IEEE Trans. Antennas Propag. 66(6), 2788–2798 (2018)
21. Hosseini, A., De Flaviis, F.: 60 GHz wideband printed quasi-parabolic reflector antenna. In: 2014 IEEE Antennas and Propagation Society International Symposium (APSURSI), pp. 1475–1476 (2014)
22. Hosseini, A., et al.: V-band high-gain printed quasi-parabolic reflector antenna with beam-steering. IEEE Trans. Antennas Propag. 65(4), 1589–1598 (2017)
23. Menéndez, L.G., et al.: 3D Printed 20/30-GHz dual-band offset stepped-reflector antenna. In: 2015 9th European Conference on Antennas and Propagation (EuCAP), pp. 1–2 (2015)
24. Zhai, Y., et al.: Ka-band lightweight high-efficiency wideband 3D printed reflector antenna. Intl. J. Antennas Propag. (2017)
25. Zhang, S., et al.: 3D-printed planar graded index lenses. IET Microw. Antennas Propag. 10(13), 1411–1419 (2016)
26. Pourahmadazar, J., et al.: A millimeter-wave fresnel zone plate lens design using perforated 3D printing material. In: 2018 IEEE MTT-S International Microwave Workshop Series on Advanced Materials and Processes for RF and THz Applications (IMWS-AMP), pp. 1–3 (2018)
27. Pizarro, F., et al.: Parametric study of 3D additive printing parameters using conductive filaments on microwave topologies. IEEE Access. 7, 106814–106823 (2019)
28. Farooqui, M.F., Kishk, A.: 3-D-printed tunable circularly polarized microstrip patch antenna. IEEE Antennas Wirel. Propag. Lett. 18(7), 1429–1432 (2019)
29. Reis, J.R., et al.: Caldeirinha: novel parabolic dish antenna for RADAR applications. In: The IET's Antennas and Propagation Conference (APC) (2019)
30. Orfanidis, S.J.: Electromagnetic Waves and Antennas. Rutgers University, New Jersey (1999–2016). http://eceweb1.rutgers.edu/~orfanidi/ewa/
31. Boussatour, G., et al.: Dielectric characterization of polylactic acid substrate in the frequency band 0.5–67 GHz. IEEE Microw. Wirel. Compon. Lett. 28(5), 374–376 (2018)
32. PLA filament 1.75mm datasheet. https://www.bq.com/pt/support/pla-premium/support-sheet (2019). Accessed 15 April 2020
33. Felício, J.M., et al.: Complex permittivity and anisotropy measurement of 3D-printed PLA at microwaves and millimeter-waves. In: 2016 22nd International Conference on Applied Electromagnetics and Communications (ICECOM), pp. 1–6 (2016)
34. Dichtl, C., et al.: Dielectric properties of 3D printed polylactic acid. Adv. Mater. Sci. Eng. 2017, 10 (2017)
35. Zechmeister, J., Lacik, J.: Complex relative permittivity measurement of selected 3D-printed materials up to 10 GHz. In: 2019 Conference on microwave techniques (COMITE), pp. 1–4 (2019)
36. Reyes, N., et al.: Complex dielectric permittivity of engineering and 3D-printing polymers at Q-band. J. Infrared Millim. Terahertz Waves. 39(11), 1140–1147 (2018). https://doi.org/10.1007/s10762-018-0528-9
37. Catarinucci, L., et al.: Microwave characterisation of polylactic acid for 3D-printed dielectrically controlled substrates. IET Microw. Antennas Propag. 11(14), 1970–1976 (2017)
38. IEEE: IEEE Standard Test Procedures for Antennas ANSI/IEEE Std 149-1979, p. 01. (1979)

How to cite this article: Reis JR, Ribeiro C, Caldeirinha RFS. Compact 3D-printed reflector antenna for radar applications at K-band. *IET Microw. Antennas Propag.* 2021;15:843–854. https://doi.org/10.1049/mia2.12095